In-plane Schottky-barrier field-effect transistors based on 1T/2H heterojunctions of transition-metal dichalcogenides

Zhi-Qiang Fan, Xiang-Wei Jiang, Jun-Wei Luo, Li-Ying Jiao, Ru Huang, Shu-Shen Li, and Lin-Wang Wang

Phys. Rev. B **96**, 165402 — Published 2 October 2017

DOI: 10.1103/PhysRevB.96.165402

In-plane Schottky-barrier field-effect transistors based on 1T/2H heterojunctions of transition-metal dichalcogenides

Zhi-Qiang Fan,[1,2] Xiang-Wei Jiang,[1,*] Jun-Wei Luo,[1] Li-Ying Jiao,[3] Ru Huang,[4] Shu-Shen Li,[1] and Lin-Wang Wang[5,†]

[1]*Institute of Semiconductors, Chinese Academy of Sciences, Beijing 100083, China.*

[2]*School of Physics and Electronic Science, Changsha University of Science and Technology, Changsha 410114, China.*

[3]*Key Lab of Organic Optoelectronics & Molecular Engineering, Department of Chemistry, Tsinghua University, Beijing 100084, China.*

[4]*Institute of Microelectronics, Peking University, Beijing 100871, China.*

[5]*Materials Science Division, Lawrence Berkeley National Laboratory, Berkeley, California 94720, USA.*

As Moore's law approaches its end, two dimensional (2D) materials are intensely studied for their potentials as one of the "More than Moore' (MM) devices. However, the ultimate performance limits and the optimal design parameters for such devices are still unknown. One common problem for the 2D material based device is the relative weak on-current. In this study, two dimensional Schottky-Barrier Field-Effect Transistors (SBFETs) consisted with in-plane hetero-junctions of 1T metallic-phase and 2H semiconducting-phase Transition-Metal Dichalcogenide (TMD) are studied following the recent experimental synthesis of such devices at much larger scale. Our *ab* initio simulation reveals the ultimate performance limits of such devices, and offers suggestions for better TMD materials. Our study shows that the Schottky-Barrier heights (SBH) of the in-plane 1T/2H contacts are smaller than the SBH of out-of-plane contacts, and the contact coupling is also stronger in the in-plane contact. Due to the atomic thickness of the mono-layer TMD, the average subthreshold swing (SS) of the in-plane TMD-SBFETs are found to be close to the limit of 60mV/dec, and smaller than that of out-of-plane TMD-SBFET device. Different TMDs are considered, and it is found that the in-plane WTe_2-SBFET provides the best performance, and it can satisfy the performance requirement of sub-10nm high performance (HP) Transistor outlined by International Technology

Roadmap for Semiconductors (ITRS), thus could be developed into a viable sub-10nm MM device in the future.

---

*xwjiang@semi.ac.cn
†lwwang@lbl.gov

1. Introduction

As the Moore's law based on Si technology is approaching to its end, new materials and new designs are intensely studied for their potentials to become "More than Moore' (MM) electronic devices in the future. In the short term, the electronic industry is also looking for technologies for transistors with channel lengths below 10 nm, thus the International Technology Roadmap for Semiconductors (ITRS) has outlined the performance parameters needed in such devices[1-3]. One very promising approach for MM devices is to use two dimensional (2D) materials [4-10]. Among different 2D materials, mono-layer Transition-Metal Dichalcogenides (TMD) are very attractive due to their direct band gaps of 1.0-2.0 eV in 2H semiconducting phase, their relative stabilities and possibilities for bipolar doping [11-16]. However, there are still some doubts for whether, ultimately, a single layer TMD FET can satisfy the ITRS device requirement, especially for its on-state current strength. For example, recent experimental studies indicated that metal/TMD contact poses a major challenge to achieve high performance transistors [17,18]. In addition, the lattice mismatch between metals and the channel TMD, and possible weak coupling between their electronic states may impair the efficiency of carrier injection, which leads to small on-state current. Thus, how to reduce the contact resistance and increase the on-state current beyond that outlined by ITRS for TMD based device is a major issue.

Depending on the arrangement of the chalcogen atoms, monolayer TMDs appear in many distinct phases such as 2H phase, 1T phase, and distorted 1T phase. For a particular TMD, the stabilities of its different phases are not same [19]. In general, the 2H phases of most TMDs are more stable than the others thermodynamically [20-22]. For example, the formation energy of the 1T phases of MoS_2 is 0.84 per formula unit higher than that of 2H phase [22]. On the other hand, related theoretical studies have

suggested that the energetically more stable phase is a distorted 2×1 reconstruction of the 1T phase [23-25]. However, recent experiments demonstrate that the 2H phase TMDs can transit to the 1T phase with the help of chemical modification [26]. A semiconductor-to-metal transition accompanies this 2H to 1T structural changes [27-29]. More excitingly, the in-plane (IP) 1T/2H hetero-junctions of MoS_2 and WSe_2 have been fabricated to form phase-engineered low-resistance contacts transistors [30-32]. It has shown that the IP 1T/2H heterojunction transistors have the much better performances that the more traditional 2H/metal contact transistors [30-32]. However, the experimental device at current stage is at the scale of μm, instead of nm, and use multiple layer TMD instead of single layer. It will thus be extremely useful to study: what is the ultimate limit in an ideal device when it is shrunk to less than 10 nm and with single layer TMD; what is the best TMD material to choose to have the best performance; and what is the determining factor for such a device. Ab initio calculations and device simulations can help to address these critical questions.

The IP 1T/2H contact is also of great fundamental interest due to the absence of interface defect, which can cause Fermi-level pinning. One important question is: what determines the band alignment at an IP 1T/2H contact? Is that determined by their alignments to the vacuum, as it was found for vertical out-of-plane (OP) contacts [13]? Besides, what is the nature of the IP 1T/2H contact itself? We found that, the IP contact is a Schottky-Barrier contact, as a result, the device is a mono-layer Schottky-Barrier Field-Effect Transistor (SBFETs). Quantum transport simulations based on density functional theory (DFT) and non-equilibrium Green's function (NEGF) method will be used to study these physical problems and to simulate the whole device I/V curve. We will also compare IP contact device with the OP contact device with the same conductive 1T phase electrode. It is found that, with the proper choice of the 1T phase materials (e.g. WTe_2), it is possible to have the on-state current to be larger than the ITRS outlined requirement for sub-10nm devices. It is also found that the IP 1T/2H heterostructure device is indeed superior than the OP contact devices, in consistent with the experimental observations.

2. Model and Simulation Approach

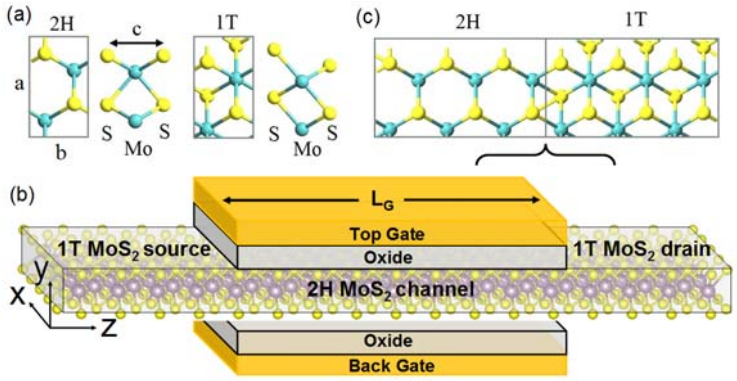

Fig. 1 (a) Atomic structures of MoS_2 rectangular unit cells with 2H and 1T phases. (b) The schematic structure of double-gated SBFET based on 1T-2H-1T mono-layer MoS_2. (c) The schematic 2H/1T interface of MoS_2.

We choose six TMD materials MX_2 (M=Mo, W; X=S, Se, Te) in our current study. The 1T-MoS_2 and 2H-MoS_2 are used here as our example. Fig. 1(a) shows the atomic structures of MoS_2 rectangular unit cells in semiconducting (2H) and metallic (1T) phases. The device of a double-gated SBFET based on 1T-2H-1T mono-layer MoS_2 is schematically shown in Fig. 1(b), where the source (S) and drain (D) are metallic 1T-MoS_2 and the channel is semiconducting 2H-MoS_2. The channel lengths (L_G) of six SBFETs are all 8.8 nm. The corresponding Equivalent Oxide Thickness (EOT=0.54 nm) and Power Supply Voltage (V_{DD}=0.72 V) follow the ITRS HP requirements. Here, EOT indicates how thick a silicon oxide film would need to be to produce the same effect as the high-k material being used, and V_{DD} is the bias voltage between source and drain. In fact, the previous experimental study showed the 1T-MoS_2 and 2H-MoS_2 could join along their zigzag edges due to the synthesis approach and growth conditions [30]. Experimental measurements and *ab* initio simulations provide a coherent physical picture of the properties of the 2D Schottky junction created at this interface [30]. For comparison, the 1T-MoS_2 and 2H-MoS_2 joining along their armchair edges is studied in our paper. The detail atomistic IP 1T/2H hetero-junction is shown in Fig. 1(c). We see that all the local tetragonal bonds between Mo and S are satisfied without any stretch. Due to the same lattice constants, 1T-MoS_2 can match with 2H-MoS_2 very well without any interfacial strains and

defects. As a result, the IP 1T/2H contacts at the source and drain region are same to each other.

The device simulations in this work are carried out by using the first-principle software package Atomistix ToolKit, which is based on density-functional theory in combination with the non-equilibrium Green's function [33]. The exchange-correlation potential is described by the local density approximation (LDA) and the wave function is expanded by the Hartwigsen-Goedecker-Hutter (HGH) basis for all atoms. The k-point samplings for calculations of bulk's electronic structures and DFT self-consistent calculations of SBFETs are 21×1×21 and 3×1×100 in the x, y and z directions, respectively. 12×1 k-point samplings in the x and y directions for the transmission calculation are the most favorable combination for the sake of more accurate results and saving computational time. The real space grid techniques are used with the energy cutoff of 200 Ry in numerical integrations. The geometries are optimized until all residual force on each atom is smaller than 0.01 eV $Å^{-1}$. When a bias voltage is applied, the current $I(V_b)$ can be calculated by the Landauer formula: $I(V_b)=\frac{2e}{h}\int T(E,V_b)[f_L(E,V_b)-f_R(E,V_b)]dE$ [34]. Here, V_b is the bias voltage, $T(E,V_b)$ is the transmission coefficient, $f_L(E,V_b)$ and $f_R(E,V_b)$ are the Fermi-Dirac distribution functions of the left and right electrodes.

3. **Results and Discussions**

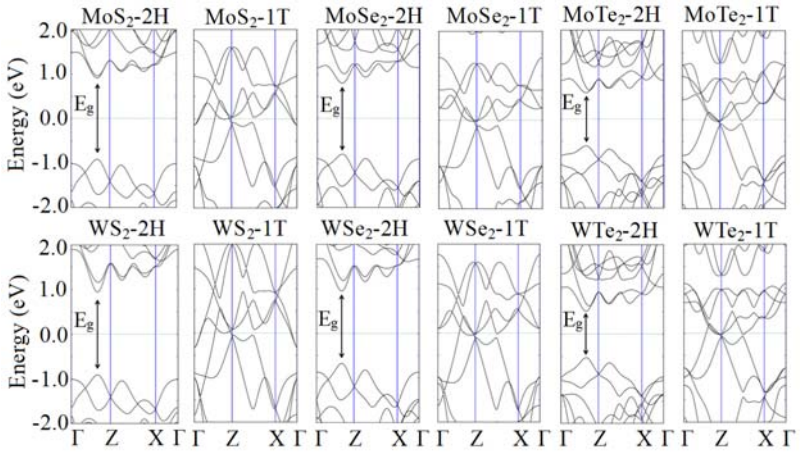

Fig. 2 Band structures of the rectangular unit cells of six TMDs with 2H and 1T phases. FL is set to zero in the energy scale.

TABLE I. Lattice constants of the rectangular cell, the calculated band-gaps (E_g) of 2H-TMDs as well as IP-Φ_{SB} and OP-Φ_{SB} of six TMD-SBFETs.

Material	a (Å)	b (Å)	c (Å)	E_g (eV)	IP-Φ_{SB} (eV)	OP-Φ_{SB} (eV)
MoS_2	5.474	3.160	3.172	1.795	0.82	0.88
$MoSe_2$	5.695	3.288	3.328	1.598	0.64	0.71
$MoTe_2$	6.094	3.518	3.605	1.195	0.44	0.46
WS_2	5.462	3.153	3.142	1.897	0.85	0.97
WSe_2	5.685	3.282	3.341	1.622	0.68	0.83
WTe_2	6.235	3.601	3.658	1.038	0.35	0.37

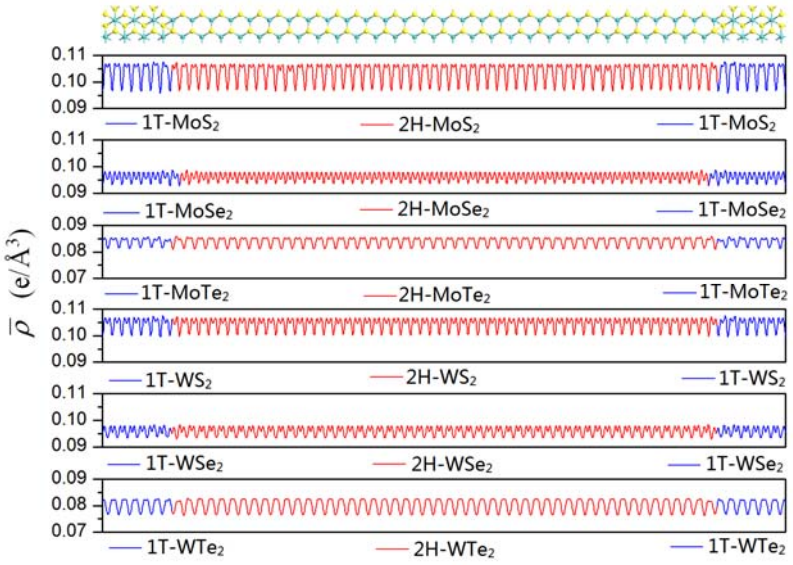

Fig. 3. The average electron density values along Z direction of six TMDs mono-layer junctions. The 1T-2H-1T MoS_2 device is also demonstrated as a schematic structure on the top of the figure.

Fig. 2 shows the calculated band structures of the rectangular unit cells of six TMDs in Fig. 1(a). All 2H phases of six TMDs are semiconductors with direct band gaps occurring along the Γ-Z direction, while all 1T phases are metals. Table I shows lattice constants of the rectangular cells and the accurate band-gaps (E_g) of 2H-TMDs, which are in good agreement with the experimental measurements and other theoretical calculations [11-16]. We did note the intrinsic band gap problem of DFT-LDA calculations, however, it is noted by several researchers that, for 2D MoS_2 and several other single-layer honeycomb structures, band gaps predicted by LDA or PBE results agree better with experimental values than GW, although the physics behind it is not clear [12,19]. The average electron density values along Z direction of six 1T-2H-1T mono-layer junctions are demonstrated in Fig. 3. Once the ribbons are

joined commensurately, *space-charge regions* form at the boundaries and determine the bending and lineup of band edges. One can see the fluctuations of the average electron density values at the 1T/2H interfaces is very small for six IP 1T-2H-1T TMDs junctions. It is also indicated the combination along their armchair edges is a good choice for the 1T/2H hetero-junction.

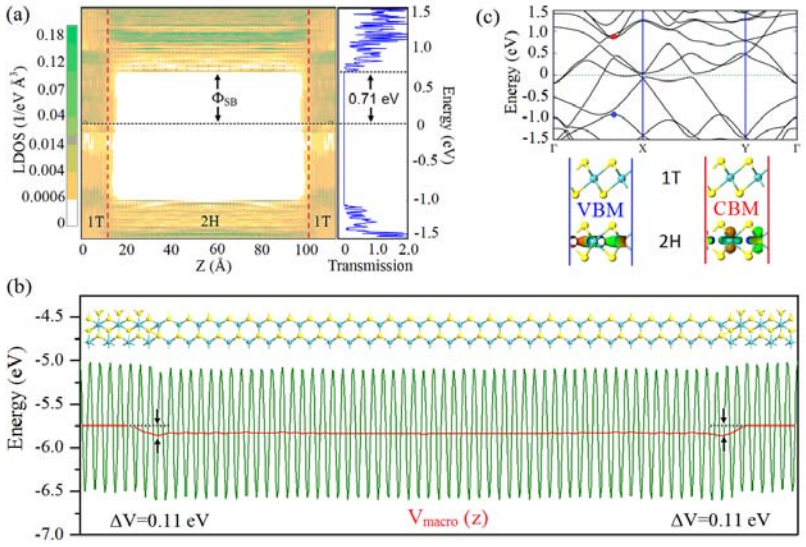

Fig. 4 (a) LDOS and transmission spectrum of 1T-2H-1T MoS_2 system under zero bias voltage. The Fermi energy is set to zero in the energy scale. (b) The averaged potential along Z direction (in turquoise) and the macroscopic average potential $V_{macro}(z)$ (in red) of 1T-2H-1T MoS_2 system under zero bias voltage. (c) Electronic band structure of OP MoS_2-1T/MoS_2-2H contact with interlayer distance 3.0 Å. The Fermi energy is set to zero in the energy scale. The VBM and CBM of the MoS_2-2H are marked by blue and red dots. Isosurfaces show the spatial distributions of the Bloch States of VBM and CBM, respectively.

The Schottky-Barrier height plays an important role in the transport properties of of SBFETs. Recent theoretical study demonstrates the linear bending of the band edges of the semiconductor at the boundary between the metal and semiconductor will affect the Schottky-Barrier height effectively [35]. Following their method, we calculate the Schottky-Barrier height of our devices from the local density states (LDOS), the transmission spectrum and the averaged potential along Z direction in Fig. 4(a) and (b). The junction of the 1T-2H-1T MoS_2 is used here as our example. First, we determine the energy difference between Fermi level (FL) of 1T-MoS_2 and the

conduction band minimum (CBM) of the 2H-MoS_2 in local density states (LDOS) or the transmission spectrum. The value is 0.71 eV. Then, we calculate its averaged potential along Z direction and the macroscopic average potential V_{macro} (z) under zero bias voltage. This way, the linear variation of V_{macro} (z) at the boundaries is reflected to linear band bending (ΔV=0.11 eV). Last, we get the real Schottky-Barrier height at the 1T/2H interface. The Schottky-Barrier height we obtained is a little different with the *ab* initio simulated result [30]. The main reason is the difference of 1T/2H contact structure which leads to different potential at the interface. The values of the IP-Φ_{SB} for six TMD-SBFETs are shown in Table I. We found that all the contacts are Schottky barrier (SB) contact with the 1T-FL located within the 2H band gap. The trend of the IP-Φ_{SB} follows that of the band-gaps: the smaller E_g corresponds to smaller IP-Φ_{SB}. For comparison, the Schottky-Barrier heights of the six OP 1T/2H contacts (OP-Φ_{SB}) are also calculated, which can be estimated by measuring the energy difference between 1T-FL and the CBM level in the 2H phase in Fig. 4(c) [13]. The interlayer distances are determined by minimizing the total energy. The OP-Φ_{SB} of OP 1T/2H contact is also shown in Table I, which is in line with the results obtained by Liu and Wei [13]. We see that, the OP 1T/2H contact having slightly larger Φ_{SB} than that of IP-Φ_{SB}. This is because the interlayer interaction can redistribute the charge density at the interface and give rise to an interface dipole between 1T/2H in the OP heterostructure, thus change the band alignment when the 1T and 2H layers become close to each other [13]. But in IP heterostructure, it is only possible to form a dipole line at the junction, which is not enough to change the alignment further away from the junction.

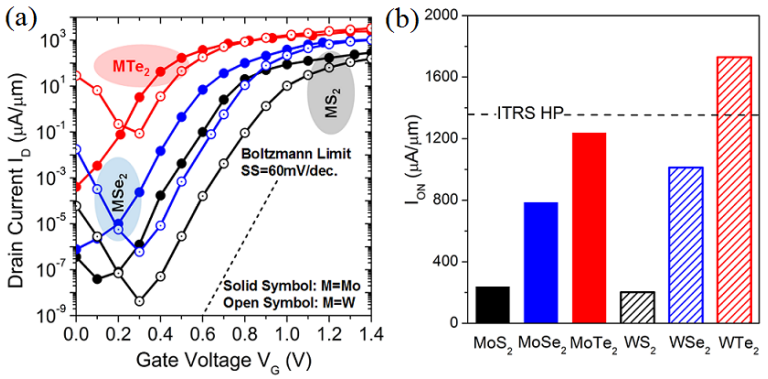

Fig. 5 (a) Transfer characteristics of MoX_2-SBFETs (solid symbol) and WX_2-SBFETs (open symbol) with 8.8 nm physical gate length (X=S, Se, Te). The dash black line is Boltzmann's thermal limit. (b) ON currents of six TMD-SBFETs. I_{ON} of ITRS HP requirement is indicated by the dash black line.

Haven studied the physics of band alignments for the 1T/2H hetero-junction, we next simulate the current transfer characteristics of the device in Fig. 1(b) by using NEGF method. Note, the Poisson equation is used to solve the potential profiles in the TMDs channel region for a given bias situation. Fig. 5(a) depicts the I-V characteristics of six IP TMD-SBFETs with 8.8 nm physical gate length. V_{DD} and EOT follow the ITRS HP 2022. The first question for the SBFET is whether the subthreshold swing (SS), which is the gate voltage needed to change the current by a factor of 10, can be close to its thermal dynamic limit of 60 meV. In a SBFET, the barrier is not at the center of the channel, instead it is at the SB itself. Although the barrier height Φ_{SB} itself will not change with the changing gate voltage, the potential profile at the other side of the SB will be changed by the gate voltage. This can change the SB thickness at a given energy level. If smaller than a given thickness, the tunneling becomes very efficient (said close to 1), so the distance from source Fermi energy to this energy level (which has the critical tunneling thickness) will become the effective barrier. This barrier can be controlled by the gate voltage. Nevertheless, due to such indirect relationship, the SBFFT usually has larger SS than the thermal dynamic limit. This can be illustrated by an approximation formula for SBFET: $SS=a_{SB}(kT/q)\ln(10)$, where $a_{SB}=1/(1-\exp(-d_{tunn}/\lambda))$ [27,28] and d_{tunn} is the SB

thickness when the tunneling become very large, and λ is an equivalent vertical thickness of the tunneling layer. Due to a_{SB}, the SS of a SBFFT is always larger than the ideal thermal dynamic limit of (kT/q)ln(10). Note that, our simulation does not rely on this approximated formula, instead it includes all tunneling and thermal distribution effects in the calculation. From our simulated results shown in Fig. 5(a), it is found that the SS's for all the TMD materials are close to the thermal dynamic limit. This is mostly because the thin vertical direction layers of TMD and oxides (~ 1-2 nm) and the relatively large d_{tunn} (~6-7 nm). This shows the true advantages of using 2D materials for FET: the efficient control of the channel potential through the gate voltage due to the thin vertical thickness.

We next consider the on-state current I_{ON}, which is often a problem for 2D FET due to the thin atomic mono-layer of the channel. The maximal drain current is inversely proportional to the Schottky-Barrier height. Indeed, due to the smallest Φ_{SB}, the I_{ON} is biggest for WTe_2-SBFET. All the I_{ON} currents are illustrated in Fig. 5(b). Here, I_{ON} is defined as the current corresponding to the gate voltage of $V_{ON}=V_{OFF}+V_{DD}$ (V_{OFF} is the gate voltage of I_{OFF} as 0.1 μA/μm). From the figure, one can see that I_{ON} is inversely correlated with the Schottky-Barrier height. The ON currents of MoS_2-SBFET and WS_2-SBFET fall far below the ITRS HP requirement (1350 μA/μm) due to the large Φ_{SB}. Only the I_{ON} of WTe_2-SBFET, being at 1729 μA/μm, is higher than the ITRS HP requirement. Thus, although the SBFET in Ref.[21] was synthesized with MoS_2, we suggest that if the same SBFET can be synthesized with WTe_2 in the future, the performance could be much better (increase I_{ON} by a factor of 7).

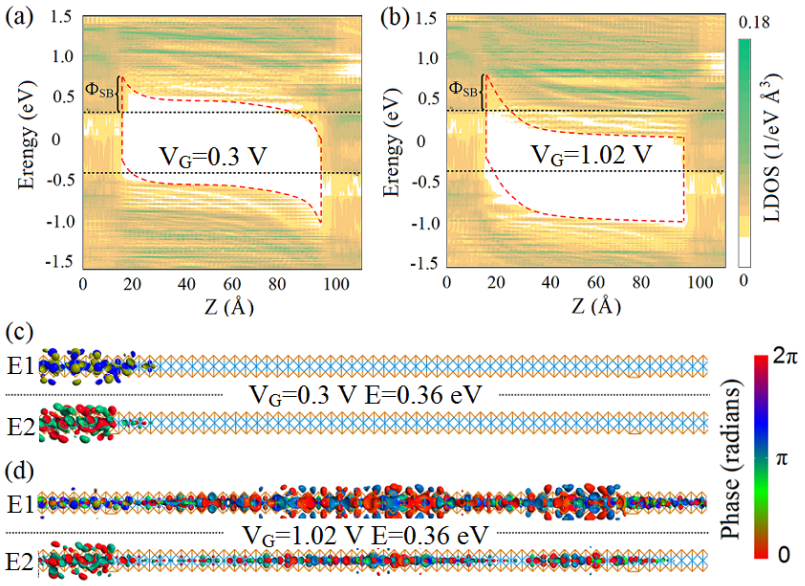

Fig. 6 LDOS of WTe_2-SBFET at the OFF state (a) and the ON state (b). Top and down black dashed lines indicate the FL of source and drain. Red dashed lines represent the schematic view of the band profile of the SBFETs. Two transmission eigenstates, E1 and E2, at the FL of source of the OFF state (c) and the ON state (d). The isovalues are fixed 0.2 for all eigenstates.

To reveal the origins for the superior performance of WTe_2-SBFET, we performed analyses on the LDOS at the OFF state (V_G=0.3 V) and the ON state (V_G=1.02 V) in Fig. 6(a) and (b). When the gate voltage is applied, the CBM of the 2H-channel region will move down gradually. At V_G=0.30 V, the drain current is minimum at I_{OFF} (0.1μA/μm). A large triangular Schottky-Barrier in Fig. 6(a) is formed due to the shift down of central LDOS, which prevents the current from tunneling through. This can also be illustrated by the transmission eigenstates at the FL of source (E=0.35 eV) in Fig. 6(c). We found the incoming wave functions of two eigenstates, E1 and E2, all localize on the sources and unable going through the central channel to reach to the drain. When the gate voltage further increases, the CBM of the center 2H channel will decrease and by-pass the FL of 1T source region, and turn on the transistor. At V_G=1.02 V, The Schottky-Barrier in Fig. 6(b) becomes much thinner and the direct tunneling through the barriers dominates the drain currents. In Fig. 6(d), the incoming wave functions of two eigenstates, E1 and E2, delocalize over the whole device including the central channel and drain. More over, the spatial distributions of the

eigenstates indicates the electron tunneling through the device mainly localizes on the transition-metal (Mo or W).

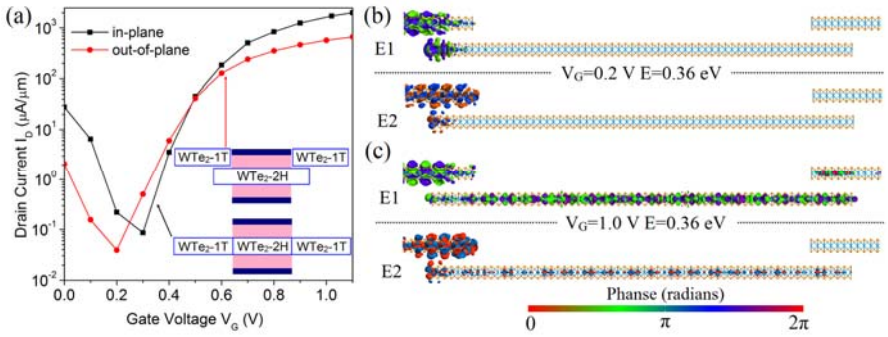

Fig. 7 (a) Transfer characteristics of IP WTe_2-SBFET and OP WTe_2-SBFET with 8.8 nm physical gate length. Two transmission eigenstates, E1 and E2, at the FL of source of the OFF state (c) and the ON state (d). The isovalues are fixed 0.2 for all eigenstates.

Finally, we compare the IP-SBFET with the more traditional OP-SBFET with 8.8 nm 2H-WTe_2 as the channel and both using 1T-WTe_2 as the source and drain electrodes. The use of the same electrode provides a more controlled comparison. Due to the contact edge effect, increasing the overlapping area will not necessarily improve the contact. Thus, we have overlapped the 2H-WTe_2 and 1T-WTe_2 with 1 nm length. EOT and V_{DD} are the same to that of IP-SBFET. The calculated I/V curve for this OP-SBFET are shown in Fig. 7(a) in comparison with that of the IP-SBFET. We see that, the performance of OP-SBFET is significantly worse than that of IP-SBFET. Not only it has lower I_{ON}, its SS is also larger. This is because in the OP-SBFET, the tunneling happens at the horizontal interface area between 2H-WTe_2 and 1T-WTe_2, and this region is outside the potential control area of the gate. Thus a short-channel effect exists, which increase the SS. On the other hand, for IP-SBFET, the tunneling place is at the edge of the gate, it is under the effective control of the gate. The smaller I_{ON} (by a factor of 4) for OP-SBFET comes from the large resistance of the current. Not only the OP-Φ_{SB} is slightly larger, the wave function coupling between 1T-layer and 2H-layer is also weaker since the electron in the 2H phase is localized at the inside layer of W, as can be seen clearly in Fig. 7(b) and (c). At OFF state, the incoming wave functions of two eigenstates, E1 and E2, all localize on the sources

and the far left of 2H-WTe_2. When the gate voltage increases to 1.0 V, the incoming wave functions of first eigenstate delocalize over the whole device including the central channel and drain. But the incoming wave functions of second eigenstate just spread to the central channel and does not reach to the drain. In contrast to all above, in the IP 1T/2H hetero junction, the coupling is due to covalent bonding and can happen at the inside layer, thus it can be much stronger.

4. Conclusion

In conclusion, we have investigated the band alignment of the 1T/2H heterjunction, both for IP and OP structures, and we have also simulated the performance of the corresponding single layer IP-SBFET. Our study shows that the Φ_{SB} of the in-plane 1T/2H contacts are smaller than the Φ_{SB} of out-of-plane contacts, and the contact coupling is also stronger in the IP case. We found that, if the WTe_2 is used, the I_{ON} can be higher than the ITRS requirement for sub 10nm devices. We also show that the IP heterostructure is indeed a better arrangement compared to the OP counterpart. Not only its SS is smaller, and close to the thermal dynamic limit, its I_{ON} is also much bigger. This is due to the effective control of the potential at the tunneling area of the Φ_{SB} in the IP arrangement, and stronger coupling of the 1T, 2H wave functions. Overall, our study shows that, WTe_2 1T/2H IP-SBFET could be a viable sub-10nm single layer device.

ACKNOWLEDGMENTS

This work was supported by the National Natural Science Foundation of China (Grant Nos. 11674039, 11574304 and 11774388), the China Postdoctoral Science Foundation (Grant No. 2016M601099), the Scientific Research Fund of Hunan Provincial Education Department (Grant No. 15A004). X. W. Jiang acknowledges the support to this work by the Youth Innovation Promotion Association CAS (grand No. 2016109) and Chinese Academy of Sciences-Peking University Pioneer Cooperation Team (CAS-PKU Pioneer Cooperation Team). L.W. W is supported by the Director, office of Science (SC), Basic Energy Science (BES), Materials Science and Engineering Division (MSED), of the US Department of Energy (DOE) under

contract No. DE-AC02-05CH11231 through the Material Theory Program (KC2301).

REFERENCES

[1] D. Xiang, H. Jeong, T. Lee, and D. Mayer, Adv. Mater. **24**, 4845 (2013).

[2] A. D. Franklin, Science **349**, 2750 (2015).

[3] D. Xiang, X. L. Wang, C. C. Jia, T. Lee, and X. F. Guo, Chem. Rev. **116**, 4318 (2016).

[4] Z. Li, J. X. Zheng, Z. Y. Ni, R. G. Quhe, Y. Y. Wang, Z. X. Gao, and J. Lu, Nanoscale **5**, 6999 (2013).

[5] X. S. Wang, H. B. Feng, Y. M. Wu, and L.Y. Jiao, J. Am. Chem. Soc. **135**, 5304 (2013).

[6] X. W. Jiang and S. S. Li, Appl. Phys. Lett. **104**, 193510 (2014).

[7] Y. H. Zhou, J. Zeng, and K. Q. Chen, Carbon **76**, 175 (2014).

[8] Á. Szabó, R. Rhyner, and M. Luisier, Phys. Rev. B **92**, 035435 (2015).

[9] Y. P. An, M. J. Zhang, D. P. Wu, Z. M. Fu, and K. Wang, J. Mater. Chem. C **4**, 10962 (2016).

[10] X. K. Chen, Z. X. Xie, W. X. Zhou, L. M. Tang, and K. Q. Chen, Appl. Phys. Lett. **109**, 023101 (2016).

[11] K. F. Mak, C. Lee, J. Hone, J. Shan, and T. F. Heinz, Phys. Rev. Lett. **105**, 136805 (2010).

[12] C. H. Chang, X. F. Fan, S. H. Lin, and J. L. Kuo, Phys. Rev. B **88**, 195420 (2013).

[13] Y. Y. Liu, P. Stradins, and S. H. Wei, Sci. Adv. **2**, 1600069 (2016).

[14] X. W. Jiang, J. Gong, N. Xu, S. S. Li, J. F. Zhang, Y. Hao, and L. W. Wang, Appl. Phys. Lett. **104**, 023512 (2014).

[15] J. H. Kang, W. Liu, D. Sarkar, D. Jena, and K. Banerjee, Phys. Rev. X **4**, 031005 (2014).

[16] Y. Y. Wang, R. X. Yang, R. G. Quhe, H. X. Zhong, L. X. Cong, M. Ye, Z. Y. Ni, Z. G. Song, J. B. Yang, J. J. Shi, J. Li, and J. Lu, Nanoscale **8**, 1179 (2016).

[17] S. Das, H. Y. Chen, A. V. Penumatcha, and J. Appenzeller, Nano Lett. **13**, 100 (2013).

[18] M. Buscema, M. Barkelid, V. Zwiller, H. S. J. van der Zant, G. A. Steele, and A. Castellanos-Gomez, Nano Lett. **13**, 358 (2013).

[19] C. Ataca, H. S ahin, and S. Ciraci, J. Phys. Chem. C **116**, 8983 (2012).

[20] K. A. N. Duerloo, Y. Li, and E. J. Reed, Nat. Commun. **5**, 4214 (2014).

[21] K. C. Santosh, C. X. Zhang, S. Hong, R. M. Wallace, and K. Cho, 2D Mater. **2**, 035019 (2015).

[22] A. Singh, S. N. Shirodkar, and U. V. Waghmare, 2D Mater. **2**, 035013 (2015).

[23] M. Calandra, Phys. Rev. B **88**, 245428 (2013).

[24] T. Hu, R. Li, and J. Dong, J. Chem. Phys. **139**, 174702 (2013).

[25] D. B. Putungan, S. H. Lin, and J. L. Kuo, Phys. Chem. Chem. Phys. **17**, 21702 (2015).

[26] A. Ambrosi, Z. Sofer, and M. Pumera, Chem. Commun. **51**, 8450 (2015).

[27] S. S. Chou, Y. K. Huang, J. Kim, B. Kaehr, B. M. Foley, P. Lu, C. Dykstra, P. E. Hopkins, C. J. Brinker, J. X. Huang, and V. P. Dravid, J. Am. Chem. Soc. **137**, 1742 (2015).

[28] Y. S. Guo, D. Z. Sun, B. Ouyang, A. Raja, J. Song, T. F. Heinz, and L. E. Brus, Nano Lett. **15**, 5081 (2015).

[29] F. Güller, A. M. Llois, J. Goniakowski, and C. Noguera, Phys. Rev. B **91**, 075407 (2015).

[30] Y. Katagiri, T. Nakamura, A. Ishii, C. Ohata, M. Hasegawa, S. Katsumoto, T. Cusati, A. Fortunelli, G. Iannaccone, G. Fiori, S. Roche, and J. Haruyama, Nano Lett. **16**, 3788 (2016).

[31] R. Kappera, D. Voiry, S. E. Yalcin, B. Branch, G. Gupta, A. D. Mohite, and M. Chhowalla, Nature Mater. **13**, 1128 (2014).

[32] Y. Q. Ma, B. L. Liu, A. Y. Zhang, L. Chen, M. Fathi, C. F. Shen, A. N. Abbas, M. Y. Ge, M. Mecklenburg, and C. W. Zhou, ACS Nano. **9**, 7383 (2015).

[33] M. Brandbyge, J. L. Mozos, P. Ordejón, J. Taylor, and K. Stokbro, Phys. Rev. B **65**, 165401 (2002).

[34] M. Büttiker, Y. Imry, R. Landauer, and S. Pinhas, Phys. Rev. B **31**, 6207 (1985).

[35] M. Aras, Ç. Kılı□, and S. Ciraci, Phys. Rev. B **95**, 075434 (2017).

[36] J. Knoch, M. Zhang, S. Mantl, and J. Appenzeller, IEEE Trans. Elect. Dev. **53**, 1669 (2006).

[37] M. Zhang, J. Knoch, J. Appenzeller, and S. Mantl, IEEE Elect. Dev. Lett. **28**, 223 (2007).